

Optical library of Ga₂O₃ polymorphs

Augustinas Galeckas,* Adrian Cernescu, Anna Kaźmierczak-Bałata, Javier García-Fernández, Calliope Bazioti, Alexander Azarov, Ji-Hyeon Park, Dae-Woo Jeon, Halin Lee, Won-Jae Lee, Rui Zhu, Zengxia Mei, Øystein Prytz, and Andrej Kuznetsov*

Gallium oxide is a novel advanced material gaining increasing attention for its unique combination of functional properties. It forms in several phases or polymorphs— α , β , γ , and κ —having variable properties because of different lattice symmetries. Optical properties are of particular importance as they determine specific device applications and can also be used for phase identification. However, a direct comparison of optical polymorph signatures, including such critical parameters as bandgaps, is challenging due to the scattered, limited, or even absent data for certain phases in the literature. To address this issue, in the present work we systematically cross-correlate optical emission and absorption features of α , β , γ , and κ thin films, as well as differently oriented β -phase bulk crystals and γ/β double polymorph structures. We demonstrate that the optical bandgap and emission features scale consistently across these polymorphs upon minimization of the methodological uncertainties. As a result, this work provides a comparative library of near- and far-field optical signatures of the polymorphs for use by the multidisciplinary research community working with gallium oxide.

1. Introduction

Gallium oxide (Ga₂O₃) is an ultra-wide bandgap semiconductor with great potential for power electronics and UV photonic applications.^[1,2] The technological importance of Ga₂O₃ is further augmented by the existence of several polymorphs, including monoclinic (β), rhombohedral (α), defective spinel (γ), and orthorhombic (κ), each possessing distinct characteristics that favor specific device applications. For instance, the higher crystal symmetry α - and κ -Ga₂O₃ phases are expected to enhance the performance of solar-blind UV optoelectronics;^[3] also promising are α -Ga₂O₃-based Schottky barrier diodes and metal-oxide-semiconductor field-effect transistors.^[4] Moreover, the spontaneous polarization,^[5,6,7] inherent to κ -Ga₂O₃ phase due to the lack of inversion symmetry, provides an opportunity for creating a two-dimensional electron gas

(2DEG) and realization of high-performance devices that rely on the 2DEG confinement.^[8,9] The monoclinic β -Ga₂O₃ presently dominates over other polymorphs in a wide range of device applications^[2,10,11,12,13] owing to its stability and well established large size single crystal wafer fabrication. Recently, the functionality of β -Ga₂O₃ has been further extended through ion irradiation-induced phase transformations.^[14,15,16] The γ -Ga₂O₃ polymorph, formed through disorder-induced ordering, demonstrates remarkably high radiation tolerance^[17] and offers an opportunity to utilize unique properties of the polymorphic γ/β heterostructure,^[18,19] thus broadening the range of applications beyond what single-phase materials can achieve. In addition to the diverse applications of crystalline polymorphs, the amorphous state of Ga₂O₃ demonstrates significant potential as well, especially in solar-blind optoelectronics^[20] and data storage technologies.^[21,22]

The current understanding of the physical properties of various polymorphs varies widely. The most comprehensive studies have been conducted on the β polymorph, whereas the γ phase remains the least explored. This trend also applies to optical emission and absorption properties, including optical bandgaps, which are often subjects of controversy in the literature. Indeed, the reported data for fundamental energy gap (E_g) of Ga₂O₃, considering all polymorphs (α , β , γ , and κ), covers the range from 4.4 to 5.6 eV.^[3,23,24,25,26,27] Meanwhile, the bandgap of monoclinic β -Ga₂O₃, determined from the onset of band-edge absorption, varies nearly as

A. Galeckas, J. García-Fernández, C. Bazioti, A. Azarov, Ø. Prytz, A. Kuznetsov
Department of Physics
Centre for Materials Science and Nanotechnology
University of Oslo
PO Box 1048 Blindern, N-0316 Oslo, Norway
E-mail: augustinas.galeckas@fys.uio.no,
E-mail: andrej.kuznetsov@fys.uio.no
A. Cernescu
attocube systems AG
85540 Haar, Germany
Anna Kaźmierczak-Bałata
Institute of Physics
Silesian University of Technology
44-100 Gliwice, Poland
Ji-H. Park, D-W. Jeon, H. Lee
Korea Institute of Ceramic Engineering & Technology
Jinju 52851, Republic of Korea
W-J. Lee
Department of Advanced Materials Engineering
Dong-Eui University
47340 Busan, Republic of Korea
R. Zhu, Z. Mei
Songshan Lake Materials Laboratory
523808 Dongguan, Guangdong, P. R. China
Institute of Physics
Chinese Academy of Sciences
100190 Beijing, P. R. China

much, ranging from 4.4 to 5.0 eV.^[28] The wide bandgap variation reported for the same polymorph is due to a combination of several methodological factors and is only partly attributable to the anisotropic crystal structure, as detailed below. Indeed, literature data for corundum-like α -Ga₂O₃, which has the widest bandgap among all polymorphs, shows a similarly wide spread of E_g values (5.0–5.6 eV).^[29,30] The optical data for κ - and γ -Ga₂O₃ are less documented compared to other polymorphs, with bandgap energies reported from 4.6 eV to 4.9 eV for κ -Ga₂O₃,^[31,32,33] and within the range of 5.0 to 5.17 eV for γ -Ga₂O₃.^[34,35] These uncertainties motivate a systematic study of the optical absorption and emission signatures of different Ga₂O₃ polymorphs in order to establish a reliable reference data repository, or optical library, which is addressed in this work.

The bandgap is commonly determined from the optical absorption edge, which, in non-cubic crystals, depends on the crystallographic direction, resulting in anisotropy. The absorption measurements typically utilize non-polarized light at normal incidence, meaning that the electric field vector \mathbf{E} of the light lies within the surface plane. For (010) oriented β -Ga₂O₃, this means that \mathbf{E} is perpendicular to the major crystallographic axis \mathbf{b} , and thus the anisotropy is negligible, as confirmed experimentally by polarization-dependent variation of bandgap $\Delta E_g \sim 0.03$ eV.^[36] By contrast, (-201) oriented β -Ga₂O₃ with the axis $\mathbf{b} = [010]$ in the surface plane exhibits strong anisotropy, as evidenced by $\Delta E_g \sim 0.2$ eV blue-shift for the light polarized along the \mathbf{b} direction.^[36] In transmittance measurements using non-polarized light, the absorption edge includes both higher- and lower-energy contributions. However, the lower-energy contribution controls the onset of the absorption edge that defines the optical bandgap, thereby ruling out anisotropy as the main cause of scattered E_g values in the literature for monoclinic β -Ga₂O₃. Regarding the anisotropy of other polymorphs, α -Ga₂O₃ is typically grown as a film on c-plane sapphire, following its symmetry. Therefore, polarization-dependent absorption is not expected. The same argument holds for γ -Ga₂O₃ due to its cubic crystal symmetry. Clearly, the widely spread bandgap values reported for different polymorphs cannot be attributed solely to anisotropy, but rather to a combination of anisotropy and a number of methodological factors. These include the variety of spectroscopic techniques used for bandgap assessment, such as ellipsometry, transmittance, reflectance and photoluminescence excitation (PLE),^[30,37,28] as well as the different analytical procedures employed, like derivative analysis, simulation, linear regression and Tauc method [α , $ah\nu$, $(ah\nu)^{1/2}$, $(ah\nu)^2$].^[38] The variations in structure (bulk crystals vs. thin films) and crystalline quality of the tested materials are also among the critical factors.

It is noteworthy that several well-established methods and techniques, in addition to conventional transmittance approach, are capable of effective polymorph characterization, each with its own limitations and challenges. For instance, ellipsometry is more surface-sensitive than others, and it is an indirect method that involves medium modeling and E_g calculation from the dispersion of complex refractive index. The PLE method relies on monitoring the emitted light while varying the photo-excitation wavelength. This implies that photo-excitation depth decreases with the increase in photon energy, making non-radiative surface recombination the

predominant pathway at shallow excitation depths. This, in turn, may distort the recorded absorption edge and thus affect the estimated E_g value. On the other hand, bandgap assessment using transmittance method imposes certain requirements for homogeneity, thickness, and surface smoothness of the medium, in effect limiting its application to thin films on transparent substrates.

In this study, transmittance spectroscopy is the method of choice to investigate polymorph-related variations of the absorption edge and to assess the optical bandgaps (E_g) of polymorphs represented by thin films (<1 μm) grown on sapphire (c-Al₂O₃). Furthermore, to illustrate the systematic discrepancies in bandgap parameters due to the structure of the tested materials, bulk (thick) crystals were characterized and compared with the data for thin films. Simultaneously, a complementary method, diffuse-reflectance spectroscopy (DRS), which can probe both thin films on homo/hetero substrates and bulk materials, was applied for a comparative evaluation of bandgap parameters. In addition, the emission properties of the polymorphs were assessed using photoluminescence (PL) spectroscopy. Finally, an insight into near-field optical signatures of the polymorphs was attained by employing scanning nanoscale Fourier Transform Infrared (nano-FTIR) spectroscopy method.

Importantly, the optical absorption and emission properties of different polymorphs were characterized using identical/fixed experimental conditions and parameter extraction routines. This approach provides reliable insights into polymorph-specific features by minimizing the uncertainties linked to a variety of bandgap assessment methods and techniques used in the literature. In particular, we systematically cross-correlate the absorption edge and photoluminescence properties of Ga₂O₃ polymorphs, including monoclinic β , corundum-like α , orthorhombic κ , and defective cubic spinel γ , as well as amorphous Ga₂O_x. By establishing a comparative library of near- and far-field optical signatures for various Ga₂O₃ polymorphs, this work aims to serve as a reference for phase identification and the recognition of polymorph-specific optical properties.

2. Results and Discussions

2.1. Structural properties

Figure 1 shows XRD 2 θ scans with indexed reflections of the α -, β -, γ and κ -Ga₂O₃ thin films on sapphire (see panels a-c) as well as the data collected for (010) β -Ga₂O₃ wafer and γ/β -Ga₂O₃ double polymorph structure in panel (d). Notably, the displayed XRD patterns validate both the crystalline quality and single-phase purity of all samples representing different Ga₂O₃ polymorphs. The uniform single-phase state of the samples throughout the entire thickness of the layers is confirmed by TEM analysis too, as illustrated by selected area electron diffraction (SEAD) patterns and cross-sectional images of the samples in Figure 2. Importantly, the phase identification in Figures 1 and 2 aligns with the findings in the literature, ensuring that the samples collectively represent a comprehensive selection for realizing the objective of this study, which is to establish an optical library for Ga₂O₃ polymorphs.

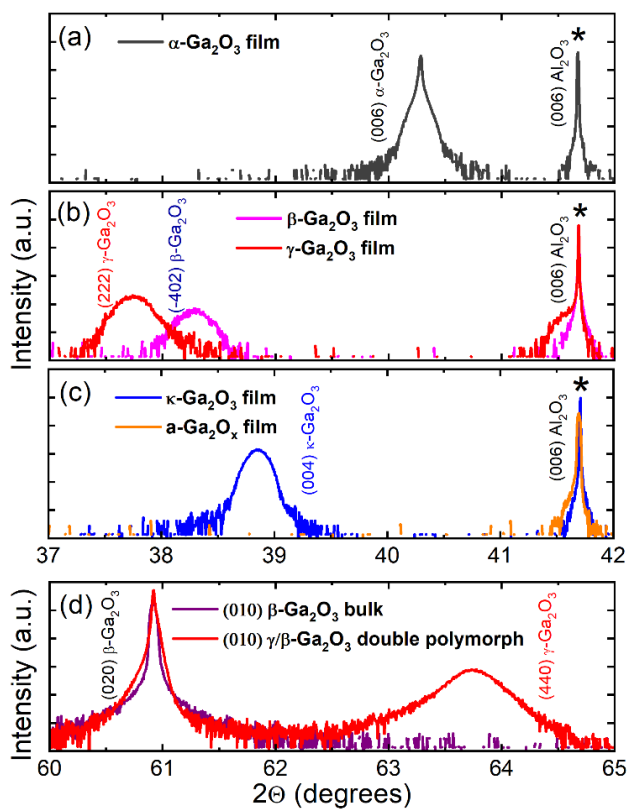


Figure 1. X-ray diffraction (XRD) spectra of the α , β , γ , and κ Ga_2O_3 polymorphs used in this study. Note that the data for amorphous ($\text{a-Ga}_2\text{O}_x$) phase in panel (c) is hidden in the background due to its low intensity.

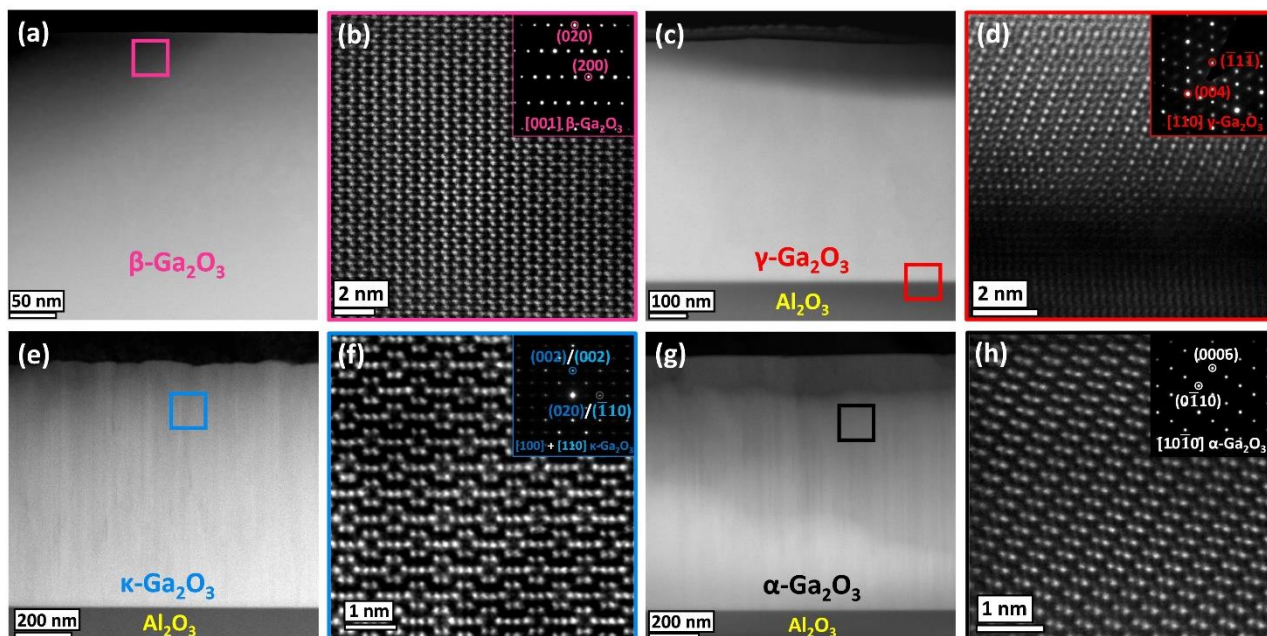


Figure 2. Low-magnification and corresponding atomic resolution HAADF STEM images for β - Ga_2O_3 (a-b), γ - Ga_2O_3 (c-d), κ - Ga_2O_3 (e-f) and α - Ga_2O_3 (g-h) polymorphs. The colored boxes in the low-magnification images indicate where the high-resolution images were acquired. The insets show the SAED along the corresponding zone axis.

2.2. Absorption properties

The single-phase α -, β - and κ -Ga₂O₃ films on sapphire as well as bulk β -Ga₂O₃ crystals permit both transmittance and diffuse-reflectance measurements for the bandgap assessment. Such a twofold approach presents an opportunity to interrelate the results of the two spectroscopic techniques, which are equally capable of characterizing the optical absorption edge, yet differ essentially in terms of probing depth. While the transmission of light invariably probes the entire medium, the diffuse-reflectance signal is largely determined by evanescent light penetration and light scattering at surface irregularities, which together lead to a higher sensitivity to near-surface properties than to bulk properties. The latter fact offers great advantages for studying multilayer structures, including γ thin films in double polymorph γ/β structures, since the diffuse-reflectance signal can be collected in a controlled manner from the near-surface region by adjusting focal plane position within the sample. In what follows, we compare the results obtained by the two

spectroscopy techniques for the different polymorph thin-films on sapphire (sample set I). Additional results, which include measurements of the bulk samples, are provided in the Supplemental Material.

Figure 3 summarizes the optical absorption and bandgap results for the α , β , γ , and κ polymorphs of Ga₂O₃, as well as amorphous Ga₂O_x, derived from diffuse-reflectance and transmittance measurements at room temperature. Herein, we follow the common method for estimating bandgaps from the fundamental absorption spectrum, based on the relation $ahv \sim (hv - E_g)^n$, where α is the absorption coefficient at photon energy hv and n depends on the type of optical transition ($n = 1/2$ for direct allowed and $n = 2$ – for indirect allowed).^[39] Accordingly, direct and indirect bandgaps can be deduced from linear interpolations of $(ahv)^2$ and $(ahv)^{1/2}$ plotted against photon energy (hv), which is a graphical analysis approach known as the Tauc method.^[40] In the case of transmittance measurements, the spectra are first transformed into absorbance ($A = \alpha d = -\ln T$), which can then be analyzed using Tauc plots, as

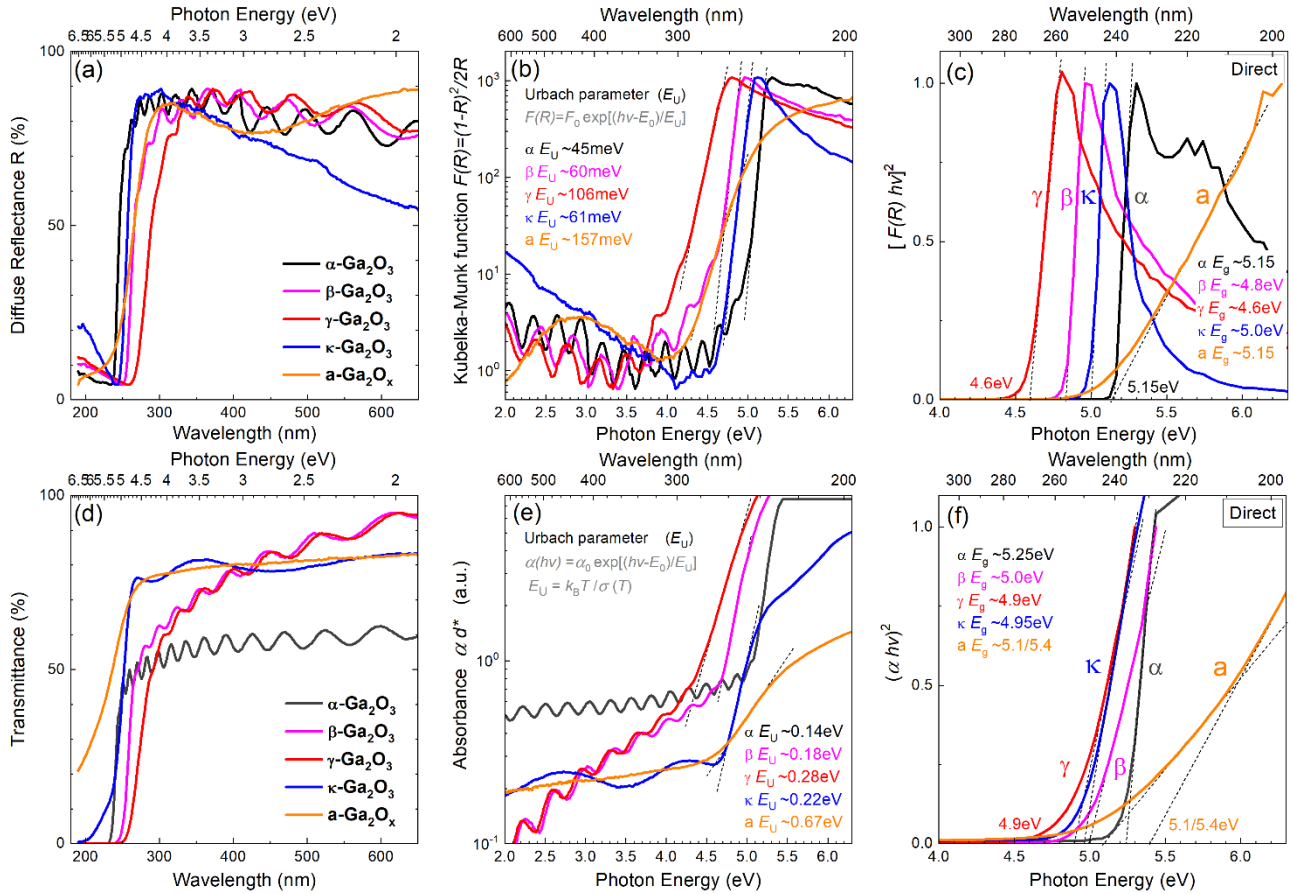


Figure 3. Optical bandgap assessment of the α , β , γ , κ Ga₂O₃ polymorphs and amorphous Ga₂O_x from diffuse-reflectance and transmittance measurements performed at room temperature: (a) Diffuse-reflectance spectra (normalized), (b) Kubelka-Munk function $F(R)$ versus incident photon energy hv , (c) Tauc plot of the modified Kubelka-Munk function $[F(R)/hv]^2$ considering direct allowed transitions. (d) Transmittance spectra (normalized), (e) Absorbance (αd^*) as a function of photon energy hv . (f) Tauc plot of the absorbance $[\alpha hv]^2$ considering direct allowed transitions. Straight lines are linear extrapolations providing the Urbach energy (E_U) (inverse of the slope in panels b, e) and bandgap (E_g) parameters (intercepts of the energy-axis in panels c, f).

shown in Figures 3d, 3e, and 3f, respectively. Similarly, the measured diffuse-reflectance values (R) are converted to the Kubelka–Munk (K-M) function, $F(R) = (1-R)^2/2R = \alpha/S$, where α is the absorption coefficient, and S is the scattering factor. Assuming S is a constant, K-M function is directly proportional to absorption coefficient, i.e., $F(R) \sim \alpha$, making the K-M spectra analogous to absorbance spectra. Thus, the Tauc method can be applied to diffuse-reflectance measurements by using a modified K-M function, $[F(R)h\nu]^2$, plotted against photon energy ($h\nu$), to assess the bandgap. Figures 3a, 3b, and 3c illustrate the three stages of the diffuse-reflectance data transformation.

In addition to estimating bandgaps from the fundamental absorption edge, we also examine the region below the energy gap, known as the Urbach tail, which is described by the exponential relation^[41] $\alpha(h\nu) = \alpha_0 \exp[(h\nu - E_0)/E_U]$. Here, E_U is the Urbach energy parameter, commonly used to quantify energy disorder at the band edges. This disorder parameter accounts for both structural disorder, which causes localized exponential-tail states, and dynamic disorder from electron-phonon scattering. In Figure 3, the absorption spectra are presented on a semilogarithmic scale; hence, E_U parameters are quantified by linear fitting of the absorption edge slopes indicating the degree of imperfection for each polymorph. The optical bandgap and Urbach energy parameters for the α -, β -, γ -, and κ -Ga₂O₃ polymorphs, as well as amorphous a-Ga₂O_x, are summarized in Table I. The values estimated from transmittance and diffuse-reflectance measurements are also plotted in Figure 4 for direct comparison. One can notice an inverse correlation between the Urbach energy E_U and the optical band gap E_g of the polymorphs. The amorphous a-Ga₂O_x exhibits the widest Urbach tail, as expected for a disordered material. Several other correlations are noteworthy when comparing the two measurement techniques.

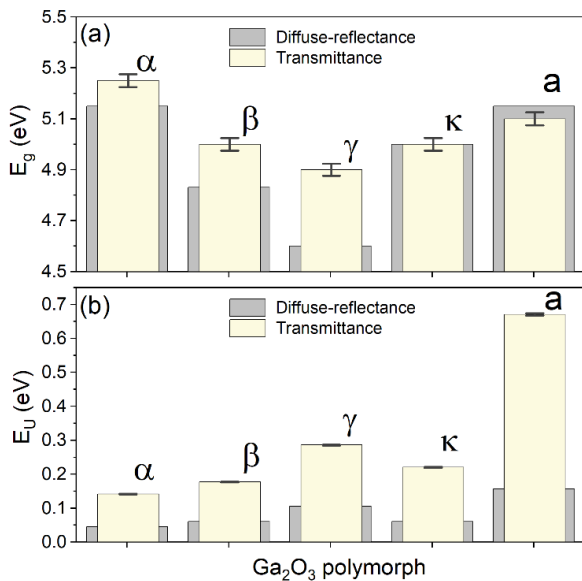


Figure 4. Comparison of (a) optical bandgap and (b) Urbach energy parameters of α , β , γ , κ Ga₂O₃ polymorphs and amorphous Ga₂O_x obtained from diffuse-reflectance and transmittance measurements.

TABLE I. Summary of optical bandgap (E_g) and Urbach (E_U) parameters estimated from diffuse-reflectance and transmittance measurements.

Polymorph	Diffuse Reflectance		Transmittance	
	E_g (eV)	E_U (meV)	E_g (eV)	E_U (meV)
α -Ga ₂ O ₃	5.15 ± 0.03	45 ± 0.6	5.25 ± 0.03	141 ± 0.7
β -Ga ₂ O ₃	4.83 ± 0.02	60 ± 0.3	5.00 ± 0.02	177 ± 0.9
γ -Ga ₂ O ₃	4.60 ± 0.02	106 ± 0.5	4.90 ± 0.02	286 ± 1.4
κ -Ga ₂ O ₃	5.00 ± 0.02	61 ± 0.3	5.00 ± 0.02	220 ± 1.1
a-Ga ₂ O _x	5.15 ± 0.02	157 ± 1.4	5.10 ± 0.03	670 ± 6.8

While polymorph-specific trends are identical, there is an apparent technique-specific discrepancy in under-/over-estimated E_g/E_U values. Additionally, there is a structure-specific trend where bulk materials consistently show lower (underestimated) bandgap E_g values compared to thin films (see data in Figures 3 and 4, and Figure S1 in the Supplemental Material). The latter factor most likely is the key contributor to the widely scattered bandgap values in the literature reports. Indeed, as previously mentioned, the most direct way of extracting the optical band gap is to determine the photon energy position at which the linear extrapolation of the absorption edge intersects the baseline. At the band-edge, the absorption coefficient (α) reaches the level of 10^5 to 10^6 cm⁻¹, thus transmission measurements of the entire interband absorption spectrum require the thickness of the media (d) to be in the range of 10 to 100 nm, considering optical depth limit $ad \leq 1$. This requirement is rarely met in practice, since optical measurements usually aim to be non-destructive by preserving the original thickness of media, which might differ by several orders of magnitude in the case of bulk crystals (wafers) compared to thin films. Consequently, the apparent onset of the absorption edge varies depending on the actual thickness of the medium. For thick (bulk) material, the bandgap estimates are influenced by the low-energy tail of the absorbance, leading to underestimated (lower) E_g values compared to those obtained for thin films. The optical bandgap and Urbach energy parameters for primary sample set (thin films) and auxiliary subset (bulk (010) and (-201) β -Ga₂O₃ wafers and γ/β double polymorph structure) are summarized in Table S1 in the Supplemental Material.

Finally, it is also noteworthy that the bandgap structure, or rather the selected type of interband optical transitions, can be potential sources of E_g uncertainty. The theoretical studies predict that the fundamental energy gap of β -Ga₂O₃ is indirect, yet due to the minor energy difference between the direct and indirect gaps (~ 30 meV), in practice it is usually regarded as a direct bandgap material.^[42,43] Following this convention, the Tauc plots for direct optical transitions are considered for the bandgap analysis in Figure 3. Alternatively, when assuming Tauc plots for indirect transitions, the extracted bandgap values are systematically lower than those for direct transitions, and the discrepancy is considerably greater than that predicted by theory. The reasons are similar to those mentioned for bulk vs. thin films, as the indirect Tauc plots tend to favor the early onset of the absorption edge by stretching that region.

2.3. Emission properties

The emission properties, such as spectral contents and quantum efficiency of photoluminescence (PL), provide an additional set of optical signatures that distinguish different Ga_2O_3 polymorphs. Figure 5 displays PL spectra measured at 10K of α , β , γ , κ Ga_2O_3 polymorphs and amorphous $\text{a-Ga}_2\text{O}_x$. Here, top panel (Figure 5a) presents normalized PL spectra of the polymorphs for a direct comparison of their emission signatures, whereas the original (raw) spectra are plotted on a semi-logarithmic scale in Figure 5b for relating their quantum efficiencies. The dominant UV emission of the α -, β -, γ - and κ - Ga_2O_3 polymorphs in the range 2.9-3.3 eV share

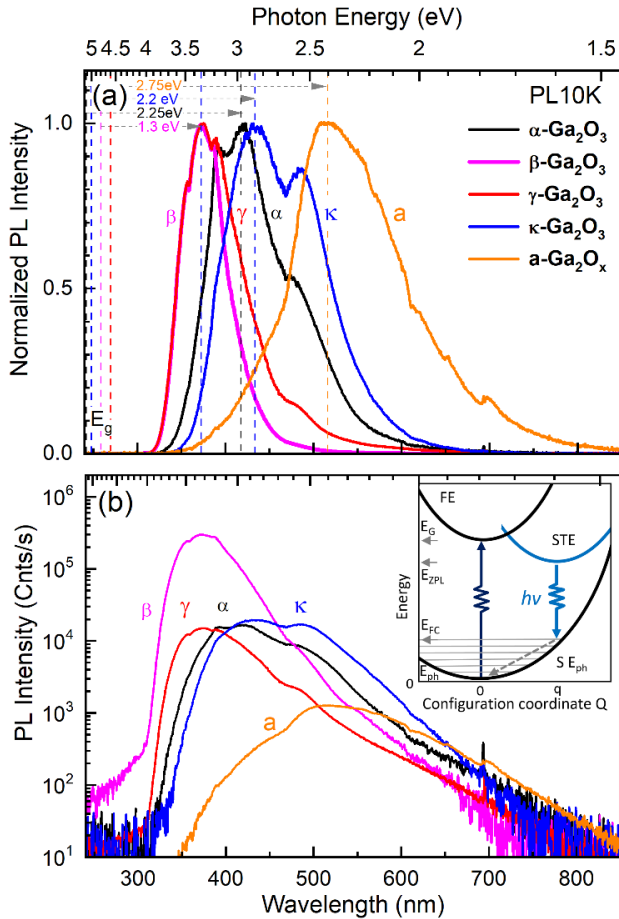


Figure 5. Photoluminescence (PL) spectra of α , β , γ , κ Ga_2O_3 polymorphs and amorphous Ga_2O_x measured at 10K: (a) normalized PL spectra presented on a linear scale for direct comparison of the characteristic emission of the polymorphs - peak position (PP) and width (FWHM); vertical dashed lines mark salient spectral features with indicated energy separation from the band-edge (Stokes shift). (b) original (raw) PL spectra on a semilogarithmic scale revealing the variance of luminescence efficiency. Inset shows a schematic diagram of the free exciton (FE) and self-trapped exciton (STE, i.e. free electron and STH) states as a function of configuration coordinate Q illustrating the origin of major Stokes shift of intrinsic emission in Ga_2O_3 polymorphs.

a common intrinsic origin linked to recombination of free electrons and self-trapped holes (STH).^[44,45,46,47] By contrast, the characteristic green luminescence (GL) of the amorphous Ga_2O_x is apparently of a different nature, most likely involving a variety of intrinsic defects (O_i , V_{Ga} and $\text{V}_{\text{Ga}}\text{-V}_0$) in donor-to-acceptor pair (DAP) recombination processes.^[48,49] This association is further supported by comparing the luminescence components and quantum efficiencies of the original (raw) PL spectra shown in Figure 5b. The amorphous $\text{a-Ga}_2\text{O}_x$ exhibits significantly, by orders of magnitude, lower quantum efficiency compared to crystalline polymorphs and apparently lacks intrinsic (STH) features. Instead, it predominantly exhibits defect-related green-red emission, which is also observed in spectra of all crystalline polymorphs, though not as a dominant characteristic.

PL results in Figure 5 reveal distinct, clearly identifiable spectral signatures for α , β , κ polymorphs, and amorphous $\text{a-Ga}_2\text{O}_x$, with β and γ phases exhibiting more closely matching signatures. The energy difference between the bandgap (E_g) and the emission peak position (PP), known as the Stokes shift (E_S), is indicated by arrows in Figure 5a. The cause of the shift for intrinsic (STH) emission is illustrated in the configuration coordinate (CC) diagram in the Inset of Figure 5b, with further details on CC models provided in Refs. [50,51]. One can observe that Stokes shift E_S scales with the bandgap E_g of a particular polymorph, i.e., β phase with the narrowest E_g (4.65 eV) also exhibits minimal E_S (1.37 eV), whereas α phase with the broadest E_g (5.15 eV) shows the largest E_S (2.25 eV).

For all polymorphs, the large Stokes shift ($E_S > 1$ eV) and broad STH emission width ($W_{\text{FWHM}} > 0.5$ eV) indicate strong electron-phonon (e - ph) coupling. This is characterized by a Huang-Rhys factor^[52] exceeding $S > 20$, as follows from the relationships^[51] $W_{\text{FWHM}} \sim 2.35 E_{\text{ph}} S^{1/2}$ and $E_S \sim E_{\text{ph}} S$ assuming the average phonon energy $E_{\text{ph}} \sim 45$ meV.^[47,53] A more accurate evaluation of e - ph coupling parameters can be achieved by fitting the STH emission as outlined below. In addition to general PL signatures of the polymorphs, such as dominant peak position and width, further analysis includes Gaussian deconvolution of emission spectra to identify overlapping components. The singled out components can then be analyzed and compared to known optical signatures from the literature. Figure 6 presents PL spectra of different polymorphs with deconvolution components color-coded and labeled in accord to common notation of Ga_2O_3 luminescence bands in literature: ultraviolet (UVL) (3.2 - 3.6 eV),^[45,46,47,54] blue (BL) (2.8 - 3.0 eV),^[55,56] green (GL) (2.4 - 2.5 eV)^[57] and red (RL) (1.7 - 1.9 eV).^[58,59,60] The fitting and emission band parameters are listed in Table II. The candidate transitions predicted by theoretical calculations^[47] are indicated by vertical markers in Figure 6d. In addition, the bold black curves in Figures 6b, 6d, and 6f show the fitting of the intrinsic STH emission component using the CC-model in the framework proposed in Ref. [61], with the parameters detailed in Table III. It is important to note that a single CC-model fit can replace several (up to three) Gaussian deconvolution components in the blue-UV region of the spectrum.

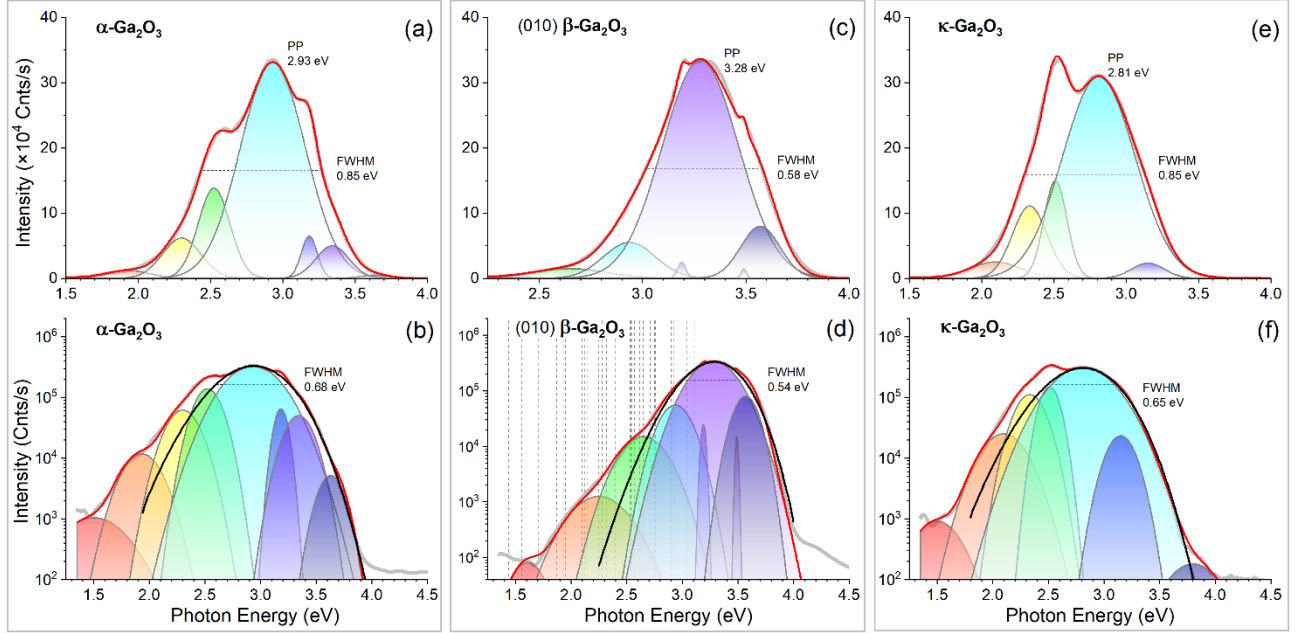


Figure 6. Deconvolution of PL spectra of rhombohedral α - Ga_2O_3 , monoclinic β - Ga_2O_3 and orthorhombic κ - Ga_2O_3 polymorphs. Representative spectra of polymorphs are plotted on linear and semi-log scales in panels (a,c,e) and (b,d,f), respectively. Gaussian deconvolution components are represented by grey curves with fitting parameters summarized in Table II. The vertical dashed lines in panel (d) are markers of the optical transitions experimentally established or theoretically predicted in the literature reports.^[54-60]

TABLE II. Gaussian deconvolution and fitting parameters of PL emission bands of α -, β - and κ - Ga_2O_3 polymorphs. The main emission components, numbered from 1 to 8, are labeled following common assignments in the literature for red (RL), green (GL), blue (BL) and ultraviolet (UVL) luminescence bands.^[54-60] PP stands for peak position, W_{FWHM} - full width at half maximum, $I(\text{norm})$ - normalized intensity of emission components.

Gaussian component / Band assignment	α - Ga_2O_3			β - Ga_2O_3			κ - Ga_2O_3		
	PP (eV)	W_{FWHM} (eV)	$I(\text{norm})$	PP (eV)	W_{FWHM} (eV)	$I(\text{norm})$	PP (eV)	W_{FWHM} (eV)	$I(\text{norm})$
1 RL	1.5	0.5875	0.00349	1.61	0.29375	1.6129E-4	1.5	0.41125	0.00206
2 RL	1.93	0.3525	0.02362	2.25	0.50525	0.00435	2.1	0.41125	0.05672
3 GL	2.3	0.31725	0.11014	2.65	0.41125	0.04225	2.33	0.282	0.17211
4 BL	2.52	0.2585	0.20409	2.94	0.29375	0.11157	2.51	0.188	0.15469
5 BL	2.93	0.52875	1	3.19	0.047	0.00792	2.81	0.5875	1
6 BL	3.18	0.12925	0.04778	3.28	0.43475	1	3.15	0.27025	0.03431
7 UVL	3.34	0.27025	0.07686	3.49	0.02938	0.00296	3.65	0.235	0
8 UVL	3.63	0.235	0.00696	3.57	0.22325	0.12265	3.8	0.47	4.64E-4

TABLE III. Effective fitting parameters of STH emission bands of α -, β - and κ - Ga_2O_3 polymorphs assuming one-dimensional configuration coordinate model:^[61] S is Huang-Rhys factor, E_0 is zero phonon line energy, E_{ph} is phonon energy, PP is peak position and W_{FWHM} - width (full width at half maximum) of the STH emission band.

Polymorph	PP (eV)	W_{FWHM} (eV)	S	E_0 (eV)	E_{ph} (meV)
α - Ga_2O_3	2.93	0.68	38.5	4.65	45
β - Ga_2O_3	3.28	0.54	24.5	4.37	45
κ - Ga_2O_3	2.81	0.65	38	4.5	45

2.4. Near-field scanning nano-FTIR analysis

The near-field optical signatures of the polymorphs were identified using scanning nanoscale Fourier Transform Infrared (nano-FTIR) spectroscopy. This involved scanning the cross-section of the double γ/β polymorph structure (Figure 7) and analyzing the plan-view surfaces of the single-phase polymorph arrangements at the nanoscale (Figure 8). The nano-FTIR technique combines scattering-type scanning near-field optical microscopy (s-SNOM) with broadband IR laser illumination and the detection of elastically scattered IR light using an interferometric Fourier transform-based scheme.^[62,63] The focusing of the broadband IR laser beam on a metallized AFM tip and the ensuing confinement of light at its apex facilitate localized near-field probing with a resolution of 10 nm. Thus, nano-FTIR enables true FTIR spectroscopy at the spatial resolution of AFM, allowing for nanoscale chemical identification and hyperspectral imaging. Referring to conventional (far-field) FTIR studies of β -Ga₂O₃, a number of bands observed in the 620 - 725 cm⁻¹ region are typically assigned to Ga-O stretching vibrations.^[54,64,65,66] Generally, a direct comparison of near-field

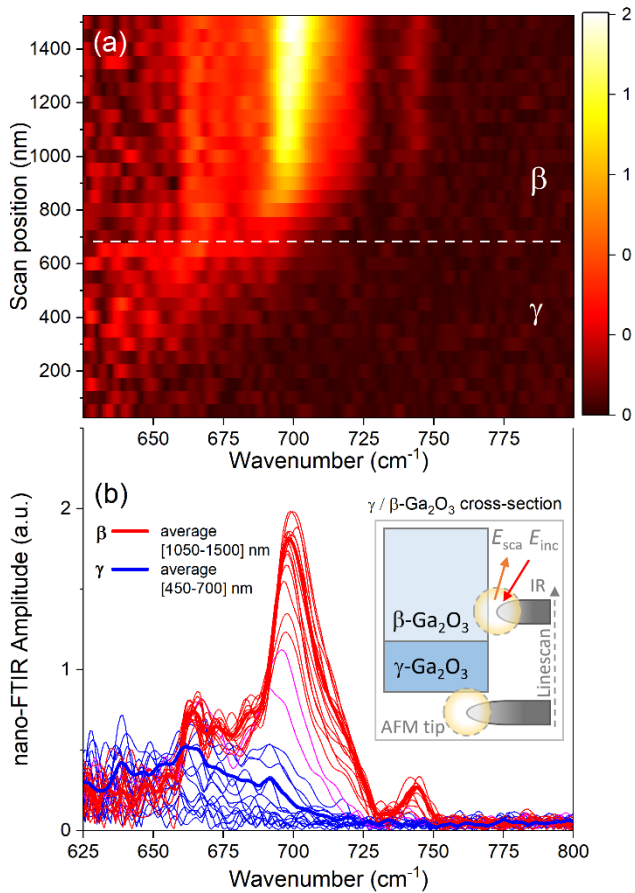


Figure 7. Nanoscale structural and spectroscopic analysis of the double γ/β -Ga₂O₃ polymorph structure by nano-FTIR: (a) 2D representation of cross-sectional nano-FTIR line scan over 1500 nm with 50 nm step. (b) Near-field optical signatures of γ and β polymorphs represented by averaged spectra in the respective domains and shown as bold lines.

and far-field FTIR fingerprints is not trivial, though it has proven effective for nonmetal materials like polymers.^[62] Nonetheless, certain insights can be gained by comparing our nano-FTIR results with the signatures of β - and κ -Ga₂O₃ polymorphs reported in Ref. [67]. The far-field FTIR signature of β -Ga₂O₃ is linked to optical phonon modes at 673, 692 and 732 cm⁻¹, which compare well with the nano-FTIR features at 666, 670, 696 and 728 cm⁻¹ in Figure 8b. The FTIR signature of κ -Ga₂O₃ is associated with a broadened peak due to several merged optical phonon modes at 715 cm⁻¹, whereas nano-FTIR demonstrates a distinct mode at 725 cm⁻¹ in Figure 8d. The near-field optical signatures in Figures 7 and 8 align with existing literature on far-field FTIR features for β and κ polymorphs, while also extending observations to a previously unreported for Ga₂O₃ nanometer-scale spatial domain. Moreover, the nano-FTIR signatures collected for all polymorphs serve as a reference point for future research, making them a valuable addition to the optical library presented in this study.

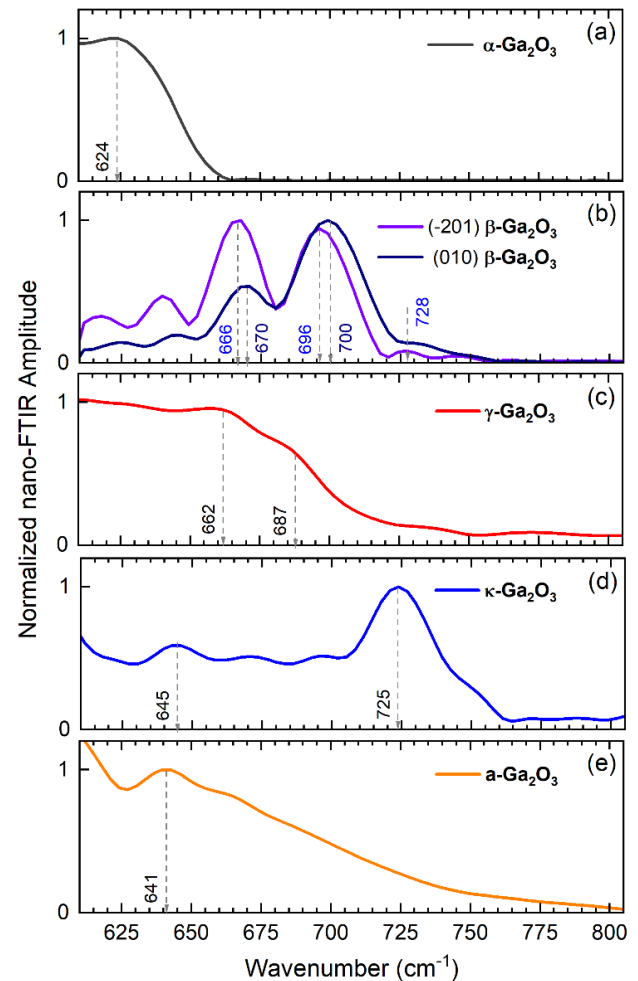


Figure 8. Near-field optical signatures obtained by nano-FTIR for α , β , γ and κ Ga₂O₃ polymorphs and amorphous a-Ga₂O_x. Vertical dashed lines are markers of the salient spectral features of the respective polymorphs.

3. Conclusion

In this work, we collected data that allows for a reliable comparison of the optical signatures of different Ga₂O₃ polymorphs. To achieve this, we cross-correlated optical emission and absorption signatures in a systematic set of thin film samples of α -, β -, γ -, and κ -phases, complemented by differently oriented β -phase bulk crystals and γ/β double polymorph structures. We demonstrate that the optical bandgap and emission features scale consistently across these Ga₂O₃ polymorphs once methodological uncertainties are minimized through systematic sample and method selection. Furthermore, the nano-FTIR signatures collected for Ga₂O₃ polymorphs for the first time serve as a reference point for future research, making them a valuable addition to the optical library presented in this study. As such, the data comprise a comprehensive collection of near- and far-field optical polymorph signatures, intended for use by the multidisciplinary research community working with Ga₂O₃.

4. Experimental Section

4.1. Samples

The representative samples of monoclinic (β), rhombohedral (α), defective spinel (γ), and orthorhombic (κ) Ga₂O₃ polymorphs studied in this work comprise thin films grown on sapphire, disorder-induced ordered layers and bulk single crystals acquired from different sources as described in what follows. The samples were categorized into two sets: primary and auxiliary. The primary set comprises polymorphs formed as thin films on transparent substrates. This configuration enables both transmittance and diffuse-reflectance analysis and the opportunity to directly compare the results:

α -Ga₂O₃ hetero-epitaxial layers (~1 μm -thick) grown by halide vapor phase epitaxy (HVPE) on *c*-axis sapphire ((0001) Al₂O₃) substrates. The details of synthesis are presented elsewhere [68].

β -Ga₂O₃ hetero-epitaxial layers (~1 μm -thick) grown by halide vapor phase epitaxy (HVPE) on *c*-axis sapphire substrates [68].

γ -Ga₂O₃ layer (~1 μm -thick) obtained by disorder-induced ordering of β -Ga₂O₃ film grown on sapphire. The irradiation with 1.5 MeV ⁵⁸Ni⁺ ions to a dose of 1×10^{16} cm⁻² was performed at room temperature.

κ -Ga₂O₃ hetero-epitaxial layers (150 nm-thick) grown by HVPE on *c*-axis sapphire ((0001) Al₂O₃) substrates.

α -Ga₂O_x amorphous (~1 μm -thick) layers deposited on *c*-axis sapphire by room-temperature RF magnetron sputtering.

The second set of samples is auxiliary and consists of bulk materials, including single crystals with various orientations and phase-transformed layers within the bulk crystals:

β -Ga₂O₃ (010), (001) and (-201) oriented β -Ga₂O₃ single crystal commercial wafers (Tamura Corp., Japan).

γ -Ga₂O₃ layers (300 nm-thick) obtained by disorder-induced ordering of (010) and (-201) β -Ga₂O₃ single crystal wafers (Tamura Corp., Japan) resulting in double polymorph γ/β Ga₂O₃ heterostructures [14].

4.2. Methods

X-ray diffraction

X-ray diffraction (XRD) 2 θ measurements were performed using the RIGAKU SmartLab diffractometer with high-resolution CuK α 1 radiation and Ge(440) four-bounced monochromator.

TEM analysis

Transmission Electron Microscopy (TEM) investigations were conducted on an FEI Titan G2 60-300 kV equipped with a CEOS DCOR probe-corrector and monochromator. Observations were performed at 200 kV and electron transparent TEM samples with a cross-sectional wedge geometry were prepared by mechanical grinding and polishing (Allied MultiPrep). Final thinning was performed by Ar ion milling with a Fishione Model 1010, and plasma cleaning was applied directly before the TEM investigations, with a Fishione Model 1020.

Transmittance and Diffuse-Reflectance Spectroscopy

Optical transmittance and diffuse-reflectance spectroscopy (DRS) measurements were performed at room temperature by employing UV-Vis-NIR spectrophotometer EVO-600 (Thermo Fisher Scientific, Inc.) equipped with Praying Mantis™ diffuse-reflection accessory (DRA), which incorporates two 90° off-axis ellipsoid mirrors that form a highly efficient illumination and collection system. The unique configuration deflects the specular reflectance away from the collecting ellipsoid, minimizing the associated spectral distortions. DRA provides results that are qualitatively similar to more common diffuse-reflectance accessory - an integrating sphere - but with the advantages of downward-looking measurement geometry, permitting horizontal mounting of samples, and collimation of probing beam to ~2 mm spot without loss of performance. Of special note is the micrometer-style height adjustment that allows for fine-tuning of the focal plane position to maximize signal from a designated sub-surface region, which is a critical feature for studies of implanted layers and stacked thin films.

The optical bandgaps of the polymorphs were estimated from the onset of the band-edge absorption by employing standard Kubelka-Munk and Tauc methods.^[40,69,70]

Photoluminescence Spectroscopy

PL spectroscopy measurements were performed at 10K temperature by employing a closed-cycle He refrigerator system (CCS-450 Janis Research, Inc.). The photo-excitation at 246 nm wavelength (5.04 eV) and 10 mW average power was provided by third-harmonic of a pulsed Ti:sapphire laser operating at 80 MHz in a femtosecond mode-locked mode (Spectra-Physics, Tsunami HP and GWU-UHG-23). PL emission was collected by a microscope and analyzed by a fiber-optic spectrometer (Avantes, AvaSpec-Mini3648-UV125) in the wavelength range 200-1100 nm with spectral resolution below 2 nm.

Scanning nano-FTIR Spectroscopy

The near-field optical signatures of the polymorphs and their structural arrangements on a nanoscale were analyzed by scanning Fourier transform infrared nano-spectroscopy (nano-FTIR) technique. Near-field nano-FTIR measurements were carried out at room temperature using a commercial IR-neaSCOPE⁴⁵ system (attocube systems AG) equipped with a broadband mid-infrared laser source and providing chemical analysis and field mapping at 10 nm spatial resolution. The nanoscale tip-enhanced IR absorption (reflection) spectra, represented by the second harmonic of the imaginary part (amplitude) of the complex spectrum, were acquired in the spectral range 620–1400 cm⁻¹ with resolution of 3 cm⁻¹ and 16 cm⁻¹.

Supporting Information

Supporting information is available from the Online Library or from the author.

Acknowledgements

The Research Council of Norway is acknowledged for the support to the Norwegian Micro- and Nano-Fabrication Facility, NorFab (project No. 295864), the Norwegian Centre for Transmission Electron Microscopy, NORTEM (project No. 197405), GOFIB (project No. 337627), and DIOGO (project No. 351033). The international collaboration was in part enabled by the INTPART Program funded by the Research Council of Norway (project No. 322382) and UTFORSK Program at the Norwegian Directorate for Higher Education and Skills (project No. UTF-2021/10210). A.K.-B. acknowledges the support from the Silesian University of Technology through a pro-quality grant, project number 14/030/SDU/10-27-01.

Conflict of Interest

The authors declare no conflict of interest.

Author Contributions

A.K. and A.G. conceptualized the work. A.A., J.H.P., D.W.J., H.L., W.J.L, R.Z., and Z.M. supplied a broad range of samples enabling this library-wide data collection. A.A. performed XRD characterization. J.G.F. and C.B. performed TEM analysis. A.G. collected optical transmission, reflection, and emission data. A.K., A.C., A.K.B., and A.G. designed and performed nano-FTIR measurements. A.G. and A.K. prepared the draft of the paper and finalized it using proposals from all coauthors. A.K., Ø.P., W.J.L., Z.M. contributed to funding acquisition and administration of their parts of the activities. All coauthors have commented and agreed on publishing the finalized manuscript..

Data Availability Statement

The data that support the findings of this study are available from the corresponding author upon reasonable request.

Keywords

gallium oxide, polymorphism, bandgap, optical characterization, photoluminescence, diffuse-reflectance, nano-FTIR

Revised: 12/18/24

1. S. J. Pearton, J. Yang, P. H. Cary IV, F. Ren, J. Kim, M. J. Tadjer, and M. A. Mastro, "A review of Ga₂O₃ materials, processing, and devices", *Appl. Phys. Rev.* 5, 011301 (2018). DOI: 10.1063/1.5006941
2. M. Higashiwaki and S. Fujita, *Gallium Oxide: Materials Properties, Crystal Growth, and Devices* (Springer Nature, 2020).
3. X. Hou, Y. Zou, M. Ding, Y. Qin, Z. Zhang, X. Ma, P. Tan, S. Yu, X. Zhou, X. Zhao, "Review of polymorphous Ga₂O₃ materials and their solar-blind photodetector applications," *J. Phys. D, Appl. Phys.* 54, 043001 (2021), DOI: 10.1088/1361-6463/abbb45
4. M. Oda, R. Tokuda, H. Kambara, T. Tanikawa, T. Sasaki and T. Hitora, "Schottky barrier diodes of corundum-structured gallium oxide showing on-resistance of 0.1 mΩ·cm² grown by MIST EPITAXY", *Appl. Phys. Express* 9 021101 (2016), DOI: 10.7567/APEX.9.021101
5. M. B. Maccioni and V. Fiorentini, "Phase diagram and polarization of stable phases of (Ga_{1-x}In_x)₂O₃", *Appl. Phys. Express* 9 , 041102 (2016). DOI: 10.7567/APEX.9.041102
6. F. Mezzadri, G. Calestani, F. Boschi, D. Delmonte, M. Bosi, and R. Fornari, "Crystal Structure and Ferroelectric Properties of ε-Ga₂O₃ Films Grown on (0001)-Sapphire", *Inorg. Chem.* 55, 12079 (2016). DOI: 10.1021/acs.inorgchem.6b02244
7. J. Kim, D. Tahara, Y. Miura, and B. G. Kim, "First-principle calculations of electronic structures and polar properties of (κ,ε)-Ga₂O₃", *Appl. Phys. Express* 11, 061101 (2018). DOI 10.7567/APEX.11.061101
8. S. B. Cho and R. Mishra, "Epitaxial engineering of polar ε-Ga₂O₃ for tunable two-dimensional electron gas at the heterointerface", *Appl. Phys. Lett.* 112 , 162101 (2018). DOI: 10.1063/1.5019721
9. P. Ranga, S. B. Cho, R. Mishra, and S. Krishnamoorthy, "Highly tunable, polarization-engineered two-dimensional electron gas in ε-AlGaO₃/ε-Ga₂O₃ heterostructures", *Appl. Phys. Express* 13, 061009 (2020). DOI: 10.35848/1882-0786/ab9168
10. M. Orita, H. Ohta, M. Hirano, and H. Hosono, "Deep-ultraviolet transparent conductive β-Ga₂O₃ thin films", *Appl. Phys. Lett.* 77, 4166 (2000). DOI: 10.1063/1.1330559
11. J. Xu, W. Zheng, and F. Huang, "Gallium oxide solar-blind ultraviolet photodetectors: a review", *J. Mater. Chem. C* 7, 8753 (2019). DOI: 10.1039/C9TC02055A
12. L. Jia, W. Zheng, and F. Huang, "Vacuum-ultraviolet photodetectors", *Photonix* 1, 22 (2020). DOI: 10.1186/s43074-020-00022-w
13. H. Xue, Q. He, G. Jian, S. Long, T. Pang, and M. Liu, "An Overview of the Ultrawide Bandgap Ga₂O₃ Semiconductor-Based Schottky Barrier Diode for Power Electronics Application", *Nanoscale Res. Lett.* 13, 290 (2018). DOI: 10.1186/s11671-018-2712-1
14. A. Azarov, C. Bazioti, V. Venkatachalapathy, P. Vajeeston, E. Monakhov, and A. Kuznetsov, "Disorder-induced ordering in gallium oxide polymorphs", *Phys. Rev. Lett.* 128, 015704 (2022). DOI: 10.1103/PhysRevLett.128.015704
15. E. A. Anber, D. Foley, A. C. Lang, J. Nathaniel, J. L. Hart, M. J. Tadjer, K. D. Hobart, S. Pearton, and M. L. Taheri, "Structural transition and recovery of Ge implanted β-Ga₂O₃", *Appl. Phys. Lett.* 117, 152101 (2020). DOI: 10.1063/5.0022170
16. T. Yoo, X. Xia, F. Ren, A. Jacobs, M. J. Tadjer, S. Pearton, and H. Kim "Atomic-scale characterization of structural damage and recovery in Sn ion-implanted β-Ga₂O₃", *Appl. Phys. Lett.* 121, 072111 (2022). DOI: 10.1063/5.0099915
17. A. Azarov, J. G. Fernández, J. Zhao, J. Zhao, F. Djurabekova, H. He, R. He, Ø. Prytz, L. Vines, U. Bektas, P. Chekhonin, N. Klingner, G. Hlawacek, A. Kuznetsov, "Universal radiation tolerant semiconductor", *Nat Commun* 14, 4855 (2023). DOI: 10.1038/s41467-023-40588-0
18. A. Y. Polyakov, A. A. Vasilev, A. I. Kochkova, I. V. Shchemerov, E. B. Yakimov, A. V. Miakonkikh, A. V. Chernykh, P. B. Lagov, Y. S. Pavlov, A. S. Doroshkevich, R. Sh. Isaev, A. A. Romanov, L. A. Alexanyan, N. Matros, A. Azarov, A. Kuznetsov and S. Pearton, "Proton damage effects in double polymorph γ/β-Ga₂O₃ diodes", *J. Mater. Chem. C*, 12, 1020 (2024). DOI: 10.1039/d3tc04171a
19. A. Abdullaev, K. Sekerbayev, A. Azarov, V. Venkatachalapathy, V. S. Chauhan, Z. Utegulov, and A. Kuznetsov, "Thermal conductivity of

- double polymorph Ga_2O_3 structures", *APL Mater.* 12, 081108 (2024). DOI: 10.1063/5.0213985
20. R. Zhu, H. L. Liang, S. G. Hu, Y. Wang, Z. X. Mei, "Amorphous- Ga_2O_3 Optoelectronic Synapses with Ultra-low Energy Consumption", *Adv. Electron. Mater.* 2022, 8, 2100741. DOI: 10.1002/aelm.202100741
 21. R. Zhu, H. Liang, S. Liu, Y. Yuan, X. Wang, F. C. Ling, A. Kuznetsov, G. Zhang, and Z. X. Mei, "Non-volatile optoelectronic memory based on a photosensitive dielectric", *Nature Communications* 14, 5396 (2023). DOI: 10.1038/s41467-023-40938-y
 22. Y. Zhang, R. Zhu, W. Huo, H. Liang, and Z. X. Mei, "Border Trap-Enhanced Ga_2O_3 Nonvolatile Optoelectronic Memory", *Nano Letters* 24, 14398 (2024). DOI: 10.1021/acs.nanolett.4c04235
 23. D. Kaur and M. Kumar, "A strategic review on gallium oxide based deep-ultraviolet photodetectors: Recent progress and future prospects," *Adv. Opt. Mater.*, vol. 9, no. 9, Mar. 2021, Art. no. 2002160, DOI: 10.1002/adom.202002160.
 24. X. Chen, F. Ren, S. Gu, and J. Ye, "Review of gallium-oxide-based solar-blind ultraviolet photodetectors," *Photon. Res.* 7 (4), 381 (2019). DOI: 10.1364/PRJ.7.000381.
 25. L. Cheng, J.-Y. Yang, and W. Zheng, "Bandgap, mobility, dielectric constant, and Baliga's figure of merit of 4H-SiC, GaN, and $\beta\text{-Ga}_2\text{O}_3$ from 300 to 620 K", *ACS Appl. Electron. Mater.* 4 (8), 4140 (2022). DOI: 10.1021/acsaelm.2c00766
 26. L. Cheng, Y. Wu, W. Zhong, D. Chen, H. Qi, and W. Zheng, "Photophysics of $\beta\text{-Ga}_2\text{O}_3$: Phonon polaritons, exciton polaritons, free-carrier absorption, and band-edge absorption," *J. Appl. Phys.* 132, 185704 (2022). DOI: 10.1063/5.0118843
 27. L. Cheng, Y. Zhu, W. Wang, and W. Zheng, "Strong electron-phonon coupling in $\beta\text{-Ga}_2\text{O}_3$: A huge broadening of self-trapped exciton emission and a significant red shift of the direct bandgap," *J. Phys. Chem. Lett.* 13, 3053 (2022). DOI: 10.1021/acs.jpclett.2c00682
 28. T. Onuma, S. Saito, K. Sasaki, T. Masui, T. Yamaguchi, T. Honda, and M. Higashiwaki, "Valence band ordering in $\beta\text{-Ga}_2\text{O}_3$ studied by polarized transmittance and reflectance spectroscopy", *Jpn. J. Appl. Phys.* 54, 112601 (2015). DOI: 10.7567/JJAP.54.112601
 29. D. Shinohara and S. Fujita, "Heteroepitaxy of Corundum-Structured $\alpha\text{-Ga}_2\text{O}_3$ Thin Films on $\alpha\text{-Al}_2\text{O}_3$ Substrates by Ultrasonic Mist Chemical Vapor Deposition", *Jpn. J. Appl. Phys.* 47 7311 (2008). DOI: 10.1143/JJAP.47.7311
 30. A. Segura, L. Artús, R. Cuscó, R. Goldhahn, and M. Feneberg, "Band gap of corundumlike $\alpha\text{-Ga}_2\text{O}_3$ determined by absorption and ellipsometry", *Phys. Rev. Materials* 1, 024604 (2017). DOI: 10.1103/PhysRevMaterials.1.024604
 31. M. Pavesi, F. Fabbri, F. Boschi, G. Piacentini, A. Baraldi, M. Bosi, E. Gombia, A. Parisini, R. Fornari, "The electronic structure of $\varepsilon\text{-Ga}_2\text{O}_3$ ", *Mater. Chem. Phys.* 205, 502 (2018). DOI: 10.1016/j.matchemphys.2017.11.023
 32. Y. Oshima, E. G. Villora, Y. Matsushita, S. Yamamoto, and K. Shimamura, "Epitaxial growth of phase-pure $\varepsilon\text{-Ga}_2\text{O}_3$ by halide vapor phase epitaxy", *J. Appl. Phys.* 118, 085301 (2015). DOI: 10.1063/1.4929417
 33. P. Mazzolini, J.B. Varley, A. Parisini, A. Sacchi, M. Pavesi, A. Bosio, M. Bosi, L. Seravalli, B. M. Janzen, M. N. Marggraf, N. Bernhardt, M. R. Wagner, A. Ardenghi, O. Bierwagen, A. Falkenstein, J. Kler, R.A. De Souza, M. Martin, F. Mezzadri, C. Borelli, R. Fornari, "Engineering shallow and deep level defects in $\kappa\text{-Ga}_2\text{O}_3$ thin films: comparing metal-organic vapour phase epitaxy to molecular beam epitaxy and the effect of annealing treatments", *Materials Today Physics*, 45, 101463 (2024). DOI: 10.1016/j.mtphys.2024.101463
 34. T. Oshima, T. Nakazono, A. Mukai, and A. Ohtomo, "Epitaxial growth of $\gamma\text{-Ga}_2\text{O}_3$ films by mist chemical vapor deposition," *J. Cryst. Growth* 359, 60 (2012). DOI: 10.1016/j.jcrysgro.2012.08.025
 35. L. E. Ratcliff, T. Oshima, F. Nippert, B. M. Janzen, E. Kluth, R. Goldhahn, M. Feneberg, P. Mazzolini, O. Bierwagen, C. Wouters, M. Nofal, M. Albrecht, J. E. N. Swallow, L. A. H. Jones, P. K. Thakur, T.-L. Lee, C. Kalha, C. Schlueter, T. D. Veal, J. B. Varley, M. R. Wagner, A. Regoutz, "Tackling Disorder in $\gamma\text{-Ga}_2\text{O}_3$ ", *Adv. Mater.* 2022, 34, 2204217. DOI: 10.1002/adma.202204217
 36. F. Ricci, F. Boschi, A. Baraldi, A. Filippetti, M. Higashiwaki, A. Kuramata, V. Fiorentini, and R. Fornari, "Theoretical and experimental investigation of optical absorption anisotropy in $\beta\text{-Ga}_2\text{O}_3$ ", *J. Phys.: Condens. Matter* 28, 224005 (2016). DOI: 10.1088/0953-8984/28/22/224005
 37. M. Meißner, N. Bernhardt, F. Nippert, B.M. Janzen, Z. Galazka, and M.R. Wagner, "Anisotropy of optical transitions in $\beta\text{-Ga}_2\text{O}_3$ investigated by polarized photoluminescence excitation spectroscopy", *Appl. Phys. Lett.* 124, 152102 (2024). DOI: 10.1063/5.0189751
 38. A. R. Zanatta, "Revisiting the optical bandgap of semiconductors and the proposal of a unified methodology to its determination", *Sci. Rep.* 9, 11225 (2019). DOI: 10.1038/s41598-019-47670-y
 39. T. P. McLean, "The absorption edge spectrum of semiconductors." *Progress in Semiconductors*, 5, 55–102 (1960).
 40. J. Tauc, R. Grigorovici, A. Vancu, "Optical Properties And Electronic Structure of Amorphous Germanium", *Phys. Status Solidi B*, 15, 627 (1966). DOI: 10.1002/pssb.19660150224
 41. F. Urbach, "The Long-Wavelength Edge of Photographic Sensitivity and Electronic Absorption of Solids", *Phys. Rev.* 92, 1324 (1953). DOI: 10.1103/PhysRev.92.1324
 42. W. Tian, H. Lu, and L. Li, "Nanoscale ultraviolet photodetectors based on one-dimensional metal oxide nanostructures", *Nano Res.* 8, 382 (2015). DOI: 10.1007/s12274-014-0661-2
 43. S. Ghose, M. S. Rahman, J. S. Rojas-Ramirez, M. Caro, R. Droopad, A. Arias, and N. Nedev, "Structural and optical properties of $\beta\text{-Ga}_2\text{O}_3$ thin films grown by plasma-assisted molecular beam epitaxy", *J. Vac. Sci. Technol. B* 34, 02L109 (2016). DOI: 10.1116/1.4942045
 44. Y. Wang, P. T. Dickens, J. B. Varley, X. Ni, E. Lotubai, and S. Sprawls, "Incident wavelength and polarization dependence of spectral shifts in $\beta\text{-Ga}_2\text{O}_3$ UV photoluminescence," *Sci. Rep.* 8(1), 18075 (2018). DOI: 10.1038/s41598-018-36676-7
 45. T. Harwig, F. Kellendonk, and S. Slappendel, "The ultraviolet luminescence of $\beta\text{-galliumsesquioxide}$ ", *J. Phys. Chem. Solids* 39, 675 (1978). DOI: 10.1016/0022-3697(78)90183-X
 46. J. B. Varley, A. Janotti, C. Franchini, and C. G. Van de Walle, "Role of self-trapping in luminescence and p-type conductivity of wide-band-gap oxides," *Phys. Rev. B* 85, 081109(R) (2012). DOI: 10.1103/PhysRevB.85.081109
 47. Y. K. Frodason, K. M. Johansen, L. Vines, and J. B. Varley, "Self-trapped hole and impurity-related broad luminescence in $\beta\text{-Ga}_2\text{O}_3$ " *J. Appl. Phys.* 127, 075701 (2020). DOI: 10.1063/1.5140742
 48. E. G. Villora, M. Yamaga, T. Inoue, G. Yabasi, Y. Masui, T. Sugawara, and T. Fukuda, "Optical spectroscopy study on $\beta\text{-Ga}_2\text{O}_3$," *Jpn. J. Appl. Phys.* 41(6A), L622 (2002). DOI: 10.1143/JJAP.41.L622
 49. Y. Berencen, Y. Xie, M. Wang, S. Prunçal, L. Rebohle, and S. Zhou, "Structural and optical properties of pulsed-laser deposited crystalline $\beta\text{-Ga}_2\text{O}_3$ thin films on silicon," *Semicond. Sci. Technol.* 34(3), 035001 (2019). DOI: 10.1088/1361-6641/aafc90
 50. A. Alkauskas, J. L. Lyons, D. Steiauf, and C. G. Van de Walle, "First-Principles Calculations of Luminescence Spectrum Line Shapes for Defects in Semiconductors: The Example of GaN and ZnO", *Phys. Rev. Lett.* 109, 267401 (2012). DOI: 10.1103/PhysRevLett.109.267401
 51. A. Alkauskas, M. D. McCluskey, and C. G. Van de Walle, "Tutorial: Defects in semiconductors - Combining experiment and theory", *J. Appl. Phys.* 119, 181101 (2016). DOI: 10.1063/1.4948245

-
52. K. Huang and A. Rhys, "Theory of light absorption and non-radiative transitions in F-centres", *Proc. R. Soc. London, Ser. A* 204, 406 (1950). DOI: 10.1098/rspa.1950.0184
53. H. Tang, N. He, Z. Zhu, M. Gu, B. Liu, J. Xu, M. Xu, L. Chen, J. Liu, X. Ouyang, "Temperature-dependence of X-ray excited luminescence of β -Ga₂O₃ single crystals", *Appl. Phys. Lett.* 115, 071904 (2019). DOI: 10.1063/1.5110535
54. Y. Wang, P. T. Dickens, J. B. Varley, X. Ni, E. Lotubai, and S. Sprawls, "Incident wavelength and polarization dependence of spectral shifts in β -Ga₂O₃ UV photoluminescence," *Sci. Rep.* 8(1), 18075 (2018). DOI: 10.1038/s41598-018-36676-7
55. T. Onuma, S. Fukioka, T. Yamaguchi, M. Sasaki, T. Masui, and T. Honda, "Correlation between blue luminescence intensity and resistivity in β -Ga₂O₃ single crystals," *Appl. Phys. Lett.* 103, 041910 (2013). DOI: 10.1063/1.4816759
56. O. M. Burdon, B. O. Bordun, I. Y. Kukharsky, and I. I. Medvid, "Photoluminescence properties of β -Ga₂O₃ thin films produced by ion-plasma sputtering," *J. Appl. Spectrosc.* 84(1), 46–51 (2017). DOI: 10.1007/s10812-017-0425-3
57. E. G. Villora, M. Yamaga, T. Inoue, G. Yabasi, Y. Masui, T. Sugawara, and T. Fukuda, "Optical spectroscopy study on β -Ga₂O₃," *Jpn. J. Appl. Phys.* 41(6A), L622 (2002). DOI: 10.1143/JJAP.41.L622
58. Q. D. Ho, T. Fraunheim, and P. Deak, "Origin of photoluminescence in β -Ga₂O₃," *Phys. Rev. B* 97, 115163 (2018). DOI: 10.1103/PhysRevB.97.115163
59. T. Huynh, E. Chikoidze, C. Irvine, M. Zakria, Y. Dumont, F. Teherani, E. Sandana, P. Bove, D. Rogers, M. Phillips, and C. Ton-That, "Red luminescence in H-doped β -Ga₂O₃," *Phys. Rev. Mater.* 4, 085201 (2020). DOI: 10.1103/PhysRevMaterials.4.085201
60. N. Gunasekar, H. MacIntyre, S. Subashchandran, P. Edwards, R. Martin, K. Daivasigamani, K. Sasaki, and A. Kuramata, "Origin of red emission in β -Ga₂O₃ analyzed by cathodoluminescence and photoluminescence spectroscopy," *Phys. Status Solidi B* 258, 2000465 (2021). DOI: 10.1002/pssb.202000465
61. M. A. Reshchikov, D. O. Demchenko, J. D. McNamara, S. Fernandez-Garrido, and R. Calarco, "Green luminescence in Mg-doped GaN", *Phys. Rev. B* 90, 035207 (2014). DOI: 10.1103/PhysRevB.90.035207
62. F. Huth, A. Govyadinov, S. Amarie, W. Nuansing, F. Keilmann, R. Hillenbrand, "Nano-FTIR Absorption Spectroscopy of Molecular Fingerprints at 20 nm Spatial Resolution", *Nano Lett.* 12, 8, 3973 (2012). DOI: 10.1021/nl301159v
63. J. M. Larson, H. A. Bechtel, R. Kostecki, "Detection and Signal Processing for Near-Field Nanoscale Fourier Transform Infrared Spectroscopy", *Adv. Funct. Mater.* 34, 2406643 (2024). DOI: 10.1002/adfm.202406643
64. S. Krehula, M. Risti, S. Kubuki, Y. Iida, M. Fabián, S. Musi, "The formation and microstructural properties of uniform α -GaOOH particles and their calcination products", *J. Alloys Compd.* 620, 217 (2015). DOI: 10.1016/j.jallcom.2014.09.134
65. I. Nowak, M. Misiewicz, M. Ziolk, A. Kubacka, V. C. Coberán, B. Sulikowski, "Catalytic properties of niobium and gallium oxide systems supported on MCM-41 type materials", *Appl. Catal. A* 325, 328–335 (2007). DOI: 10.1016/j.apcata.2007.02.029
66. S. Kumar, C. Tessarek, S. Christiansen, R. Singh, "A comparative study of β -Ga₂O₃ nanowires grown on different substrates using CVD technique", *J. Alloys Compd.* 587, 812 (2014). DOI: 10.1016/j.jallcom.2013.10.165
67. S. A. Dereshgi, J. Lee, D. Ceneda, M. C. Larciprete, M. Centini, M. Razeghi, K. Aydin, "MOCVD-grown Ga₂O₃ thin films for polarization-sensitive infrared photonics", *APL Mater.* 12 011125 (2024). DOI: 10.1063/5.0177705
68. H. Son and D.-W. Jeon, "Optimization of the growth temperature of α -Ga₂O₃ epilayers grown by halide vapor phase epitaxy," *J. Alloys Compd.* 773, 631 (2019). DOI: 10.1016/j.jallcom.2018.09.230
69. P. Kubelka, F. A. Munk, "Contribution to the Optics of Pigments", *Z. Technol. Phys.* 12, 593 (1931).
70. P. Makuła, M. Pacia, and W. Macyk, "How To Correctly Determine the Band Gap Energy of Modified Semiconductor Photocatalysts Based on UV-Vis Spectra", *J. Phys. Chem. Lett.* 9, 6814 (2018). DOI: 10.1021/acs.jpcclett.8b02892

Supplementary Material

Optical library of Ga₂O₃ polymorphs

Augustinas Galeckas,^{1,a)} Adrian Cernescu,² Anna Kaźmierczak-Bałata,³ Javier García-Fernández,¹ Calliope Bazioti,¹ Alexander Azarov,¹ Ji-Hyeon Park,⁴ Dae-Woo Jeon,⁴ Halin Lee,⁵ Won-Jae Lee,⁵ Rui Zhu,^{6,7} Zengxia Mei,^{6,7} Øystein Prytz,¹ and Andrej Kuznetsov¹

¹ University of Oslo, Department of Physics, Centre for Materials Science and Nanotechnology, PO Box 1048 Blindern, 0316 Oslo, Norway

² attocube systems AG, 85540 Haar, Germany

³ Institute of Physics, Silesian University of Technology, 44-100 Gliwice, Poland

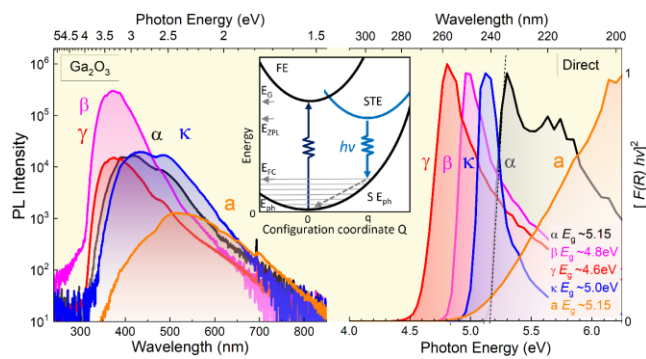
⁴ Korea Institute of Ceramic Engineering & Technology, Jinju 52851, Republic of Korea

⁵ Dong-Eui University, Department of Advanced Materials Engineering, 47340 Busan, Republic of Korea

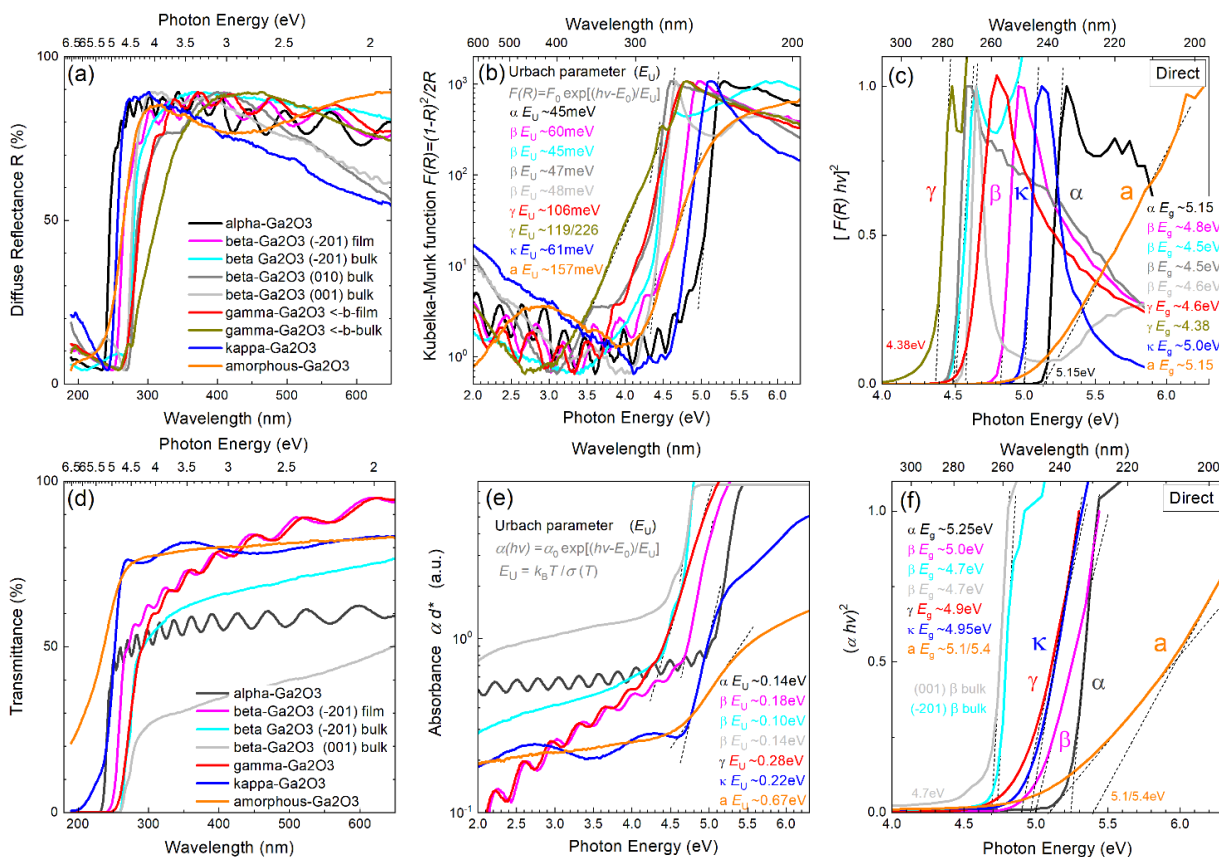
⁶ Songshan Lake Materials Laboratory, 523808 Dongguan, Guangdong, P. R. China

⁷ Institute of Physics, Chinese Academy of Sciences, 100190 Beijing, P. R. China

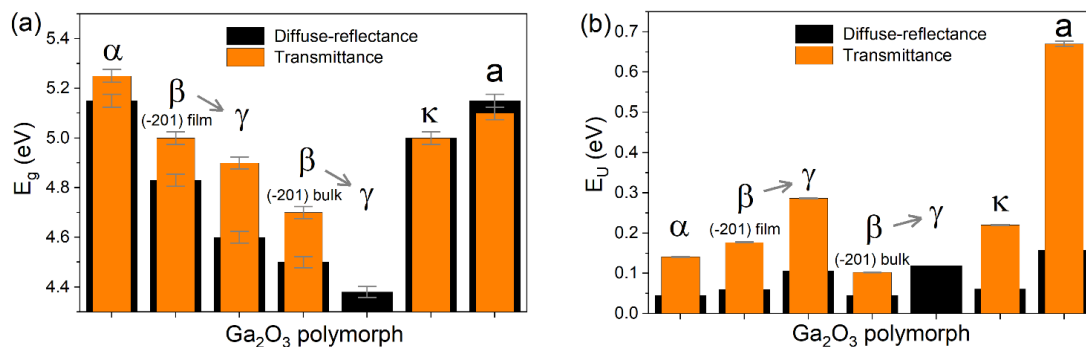
Authors to whom correspondence should be addressed: ^{a)} augustinas.galeckas@fys.uio.no, ^{b)} andrej.kuznetsov@fys.uio.no



Supplement #1: Absorption properties (RT% all samples)



Supplementary Figure S1. Optical bandgap assessment of the α , β , γ , κ Ga₂O₃ polymorphs and amorphous Ga₂O_x from diffuse-reflectance and transmittance measurements performed at room temperature: (a) Diffuse-reflectance spectra (normalized), (b) Kubelka-Munk function $F(R)$ versus incident photon energy $h\nu$, (c) Tauc plot of the modified Kubelka-Munk function $[F(R)hv]^2$ considering direct allowed transitions. (d) Transmittance spectra (normalized), (e) Absorbance (αd^*) as a function of photon energy $h\nu$. (f) Tauc plot of the absorbance $[\alpha hv]^2$ considering direct allowed transitions. Straight lines are linear extrapolations providing the Urbach energy (E_U) (inverse of the slope in panels b, e) and bandgap (E_g) energy parameters (intercepts of the energy-axis in panels c, f).

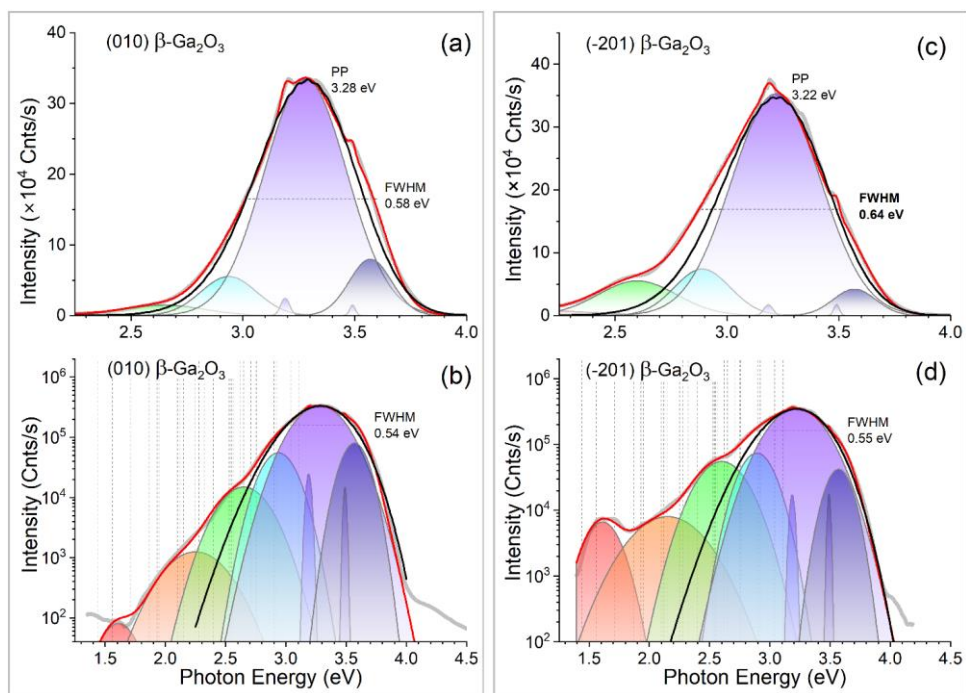


Supplementary Figure S2. Comparison of (a) optical bandgap and (b) Urbach energy parameters of α , β , γ , κ Ga₂O₃ polymorphs and amorphous Ga₂O_x obtained from diffuse-reflectance and transmittance measurements.

TABLE SI. Summary of optical bandgap (E_g) and Urbach (E_U) parameters estimated from diffuse-reflectance and transmittance measurements.

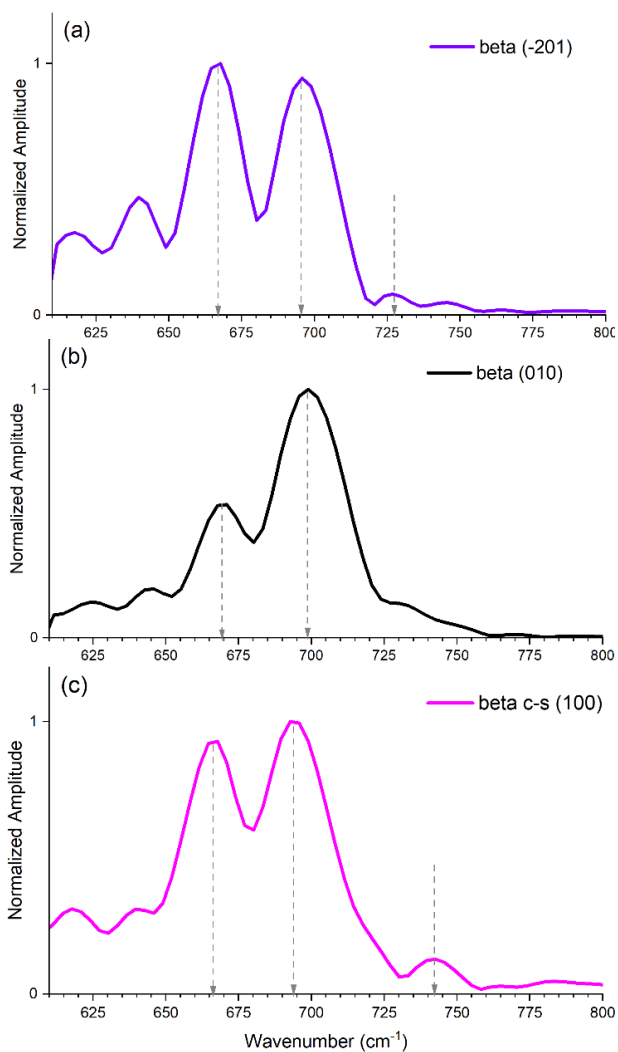
Polymorph / structure	Diffuse Reflectance		Transmittance	
	E_g (eV)	E_U (meV)	E_g (eV)	E_U (meV)
α -Ga ₂ O ₃ film	5.15 ± 0.03	45 ± 0.6	5.25 ± 0.03	141 ± 0.7
β -Ga ₂ O ₃ (-201) film	4.83 ± 0.02	60 ± 0.3	5.00 ± 0.02	177 ± 0.9
β -Ga ₂ O ₃ (-201) bulk	4.50 ± 0.02	45 ± 2	4.70 ± 0.02	102 ± 0.5
β -Ga ₂ O ₃ (010) bulk	4.50 ± 0.02	47 ± 0.9		
β -Ga ₂ O ₃ (001) bulk	4.60 ± 0.02	48 ± 0.9	4.70 ± 0.02	137 ± 0.7
γ -Ga ₂ O ₃ film	4.60 ± 0.02	106 ± 0.5	4.90 ± 0.02	286 ± 1.4
γ/β -Ga ₂ O ₃ bilayer	4.38 ± 0.02	119 ± 0.6		
κ -Ga ₂ O ₃ film	5.00 ± 0.02	61 ± 0.3	5.00 ± 0.02	220 ± 1.1
a-Ga ₂ O _x film	5.15 ± 0.02	157 ± 1.4	5.10 ± 0.03	670 ± 6.8

Supplement #2: Emission properties (PL/ bulk)

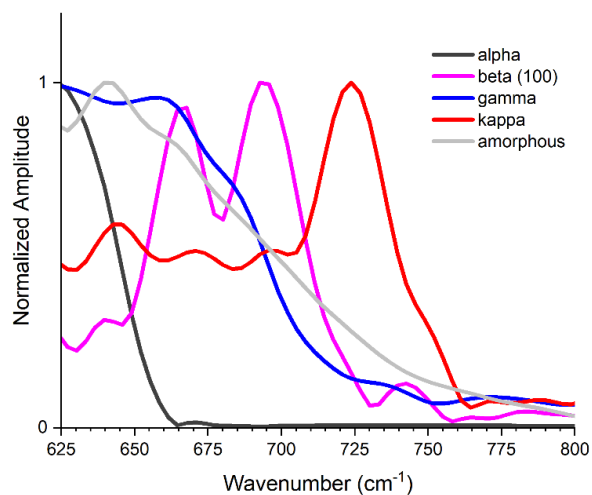


Supplementary Figure S3. PL spectra of monoclinic β -Ga₂O₃ polymorph obtained at 10K from (010) and (-201) oriented single-crystals plotted on linear and semi-log scales in panels (a,b) and (c,d), respectively. Gaussian deconvolution components are represented by grey curves. Vertical dashed lines are markers of the optical transitions (experimentally established or theoretically predicted) in the literature reports (see Table SI).

Supplement #3: Near-field scanning nanoFTIR



Supplementary Figure S4. Nano-FTIR spectra obtained at 300K for different crystal orientations of β -Ga₂O₃.



Supplementary Figure S5. Nano-FTIR spectra obtained at 300K for α , β , and κ polymorphs and amorphous Ga₂O₃.